LETTERS

A molecular molybdenum-oxo catalyst for generating hydrogen from water

Hemamala I. Karunadasa[1,2], Christopher J. Chang[1,2,3] & Jeffrey R. Long[1,2]

A growing awareness of issues related to anthropogenic climate change and an increase in global energy demand have made the search for viable carbon-neutral sources of renewable energy one of the most important challenges in science today[1]. The chemical community is therefore seeking efficient and inexpensive catalysts that can produce large quantities of hydrogen gas from water[1–7]. Here we identify a molybdenum-oxo complex that can catalytically generate gaseous hydrogen either from water at neutral pH or from sea water. This work shows that high-valency metal-oxo species can be used to create reduction catalysts that are robust and functional in water, a concept that has broad implications for the design of 'green' and sustainable chemistry cycles.

Hydrogen has emerged as an attractive candidate for a clean, sustainable fuel[2] and underpins the intense interest in creating artificial systems that use catalysts based on elements abundant in the Earth to achieve efficient hydrogen production from water[1,3–7]. Hydrogenase enzymes possessing iron and/or nickel cofactors evolve H_2 catalytically from neutral aqueous solution at its thermodynamic potential with turnover frequencies of 100 to 10,000 moles of H_2 per mole of catalyst per second[8–10]. However, the large size and relative instability under aerobic, ambient conditions of these enzymes has led to the search for well-defined molecular complexes that can produce H_2 from water in a non-biological setting.

Many examples of air- and moisture-sensitive synthetic iron–sulphur clusters have provided valuable insights into hydrogenase structure and reactivity, although they catalyse proton reduction from acids in organic solvents at fairly negative potentials of –0.9 to –1.8 V versus SHE (standard hydrogen electrode)[7,10–13]. Metal complexes that evolve H_2 at more positive potentials also still require organic acids, additives or solvents[3,4,14–18]. Although precious metals can show high catalytic activity for water reduction at low overpotential, the high cost prohibits their widespread use. The creation of Earth-abundant molecular systems that produce H_2 from water with high catalytic activity and stability thus remains a significant basic science challenge. We now report a simple molybdenum-oxo complex that catalyses the generation of hydrogen from neutral buffered water or even sea water with a turnover frequency of 2.4 moles of H_2 per mole of catalyst per second and a turnover number of 6.1×10^5 moles of H_2 per mole of catalyst. This metal-oxo complex represents a distinct molecular motif for reduction catalysis that has high activity and stability in water.

The molybdenum-oxo catalyst was discovered while we were investigating the second-row transition-metal chemistry of the pentadentate ligand 2,6-bis(1,1-bis(2-pyridyl)ethyl)pyridine ($PY5Me_2$). Metallation of $PY5Me_2$ with $MoI_2(CO)_3(MeCN)_2$ produces an 87% yield of $[(PY5Me_2)MoI]I_2$ (compound **1**). As shown by the crystal structure of compound **1** (Supplementary Fig. 1), the $PY5Me_2$ ligand enforces a pseudo-octahedral geometry around the Mo(III) centre, with the metal lying just 0.162 Å above the mean plane of the four equatorial N atoms. The plane of the axial pyridine ligand makes a nearly orthogonal angle of 81° with the plane of the equatorial N atoms, whereas analogous complexes involving first-row transition metals display much more acute angles in the range 57°–65° (ref. 19). This structure suggests increased orbital overlap and enhanced σ- and π-bonding between the second-row transition metal and the ligand. The cyclic voltammogram of compound **1** in acetonitrile shows a sequence of three reversible redox events centred at half-wave potentials of $E_{1/2} = -0.287$, –0.799 and –1.321 V versus SHE, corresponding to the $[(PY5Me_2)MoI]^{2+/1+}$, $[(PY5Me_2)MoI]^{1+/0}$, and $[(PY5Me_2)MoI]^{0/1-}$ couples, respectively (Supplementary Fig. 2). Additional peaks are associated with the redox-active iodide counter-ions, as confirmed by their absence in the cyclic voltammogram of the ion-exchanged compound $[(PY5Me_2)MoI](PF_6)_2$ (compound **2**), as well as by their presence in the cyclic voltammogram of a solution of pure iodine. Thus, $[(PY5Me_2)MoI]^{2+}$ possesses a remarkable redox flexibility, with four different redox states accessible within a window of just over 1 V.

Water reacts with orange $[(PY5Me_2)MoI]I_2$ to release hydrogen and generate a green molybdenum-oxo complex, as isolated in $[(PY5Me_2)MoO]I_2$ (compound **3**). Carrying out the reaction in an O_2-free atmosphere with $H_2{}^{18}O$ yields $[(PY5Me_2)Mo^{18}O]I_2$, with the expected isotopic $\nu_{Mo=O}$ stretching frequency shift from 961 cm^{-1} to 918 cm^{-1}. The two-electron reductive cleavage of water to release H_2 implies that $[(PY5Me_2)MoO]^{3+}$ is initially formed and subsequently reduced to $[(PY5Me_2)MoO]^{2+}$ by iodide. The viability of this process is supported by the cyclic voltammogram of compound **3**, which displays reversible $[(PY5Me_2)MoO]^{3+/2+}$ and $[(PY5Me_2)MoO]^{2+/1+}$ couples at $E_{1/2} = 1.402$ and -0.829 V versus SHE, respectively, bracketing the iodide redox chemistry, as well as by the electronic absorption spectrum of the reaction mixture, which shows the characteristic bands for iodine. To access a cleaner two-electron reaction with water, the Mo(III) compound $[(PY5Me_2)Mo(CF_3SO_3)](CF_3SO_3)_2$ (compound **4**) was reduced with one equivalent of KC_8 to yield $[(PY5Me_2)Mo(CF_3SO_3)](CF_3SO_3)$ (compound **5**). As depicted in Fig. 1, the crystal structure of compound **4** contains a pseudo-octahedral triflate complex with a Mo(II)–O distance of 2.117(9) Å. Reaction with water indeed affords $[(PY5Me_2)MoO](CF_3SO_3)_2$ (compound **6**) with the concomitant evolution of H_2, demonstrating the ability of a Mo(II)–$PY5Me_2$ complex to reduce water and eliminate H_2. The crystal structure of compound **6** confirms a pseudo-octahedral Mo(IV)-oxo complex with a short Mo–O bond of 1.685(9) Å.

The observations that $[(PY5Me_2)Mo(CF_3SO_3)]^{1+}$ can cleave water to generate H_2 and that $[(PY5Me_2)MoO]^{2+}$ can undergo multiple reductive processes led us to test the Mo(IV)-oxo complex in an electrochemical cycle for generating hydrogen from water. For ease of synthesis and to avoid the redox chemistry associated with iodide,

[1]Department of Chemistry, University of California, Berkeley, California 94720, USA. [2]Chemical Sciences Division, Lawrence Berkeley National Laboratory, Berkeley, California 94720, USA. [3]Howard Hughes Medical Institute, University of California, Berkeley, California 94720, USA.

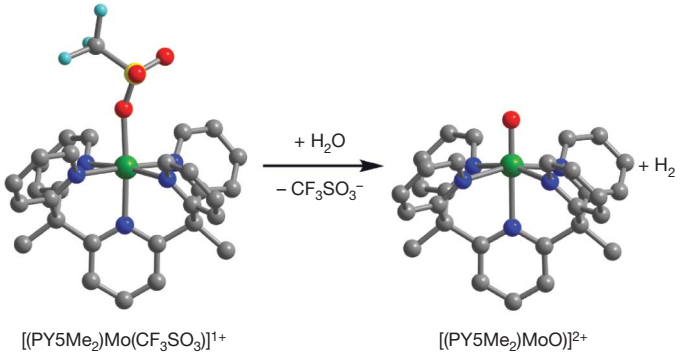

Figure 1 | Reaction of $[(PY5Me_2)Mo(CF_3SO_3)]^{1+}$ with water to form $[(PY5Me_2)MoO]^{2+}$ and release H_2. The generation of H_2 was confirmed by mass spectrometry, and the oxo ligand was shown to originate from water through observation of the expected isotopic shift for $\nu_{Mo=O}$ in the infrared spectrum, using $H_2{}^{18}O$. The structures depicted are the results of single-crystal X-ray analyses of compounds **5** and **6**, with green, yellow, light blue, red, blue and grey spheres representing Mo, S, F, O, N and C atoms, respectively; H atoms are omitted for clarity. Selected interatomic distances and angles for compounds **5** and **6** are as follows. Mo–O: 2.117(9) Å, 1.685(9) Å; mean Mo–$N_{equatorial}$: 2.14(2) Å, 2.154(3) Å; Mo–N_{axial}: 2.097(9) Å, 2.297(8) Å; mean O–Mo–$N_{equatorial}$: 93(3)°, 98(1)°; O–Mo–N_{axial}: 176.2(4)°, 179(1)°; mean $N_{equatorial}$–Mo–$N_{equatorial}$: 90(10)°, 89(8)°.

these experiments were performed using $[(PY5Me_2)MoO](PF_6)_2$ (compound **7**) obtained via reaction of compound **3** with $TlPF_6$. The cyclic voltammogram of compound **7** (Fig. 2b) indeed matches that of compound **3** minus the iodide redox chemistry. Beyond the reversible $[(PY5Me_2)MoO]^{2+/1+}$ couple, a sequence of three irreversible reduction peaks is observed. The first of these waves, at –1.301 V, presumably corresponds to formation of the neutral Mo(II) complex $[(PY5Me_2)MoO]$, which undergoes a further reaction on the timescale of the experiment. The cyclic voltammogram of compound **7** in 1 M aqueous KCl displays a quasi-reversible $[(PY5Me_2)MoO]^{2+/1+}$ couple centred at $E_{1/2} = -0.58$ V, followed by an irreversible reduction at –1.06 V (Fig. 2c). Formation of the putative Mo(II) species precedes a sharp rise in current at –1.15 V, indicating a catalytic process for water activation; mass spectrometry confirms that H_2 is evolved from these experiments. Subsequent measurements were performed in phosphate supporting electrolytes buffered to pH 7. At a scan rate of 100 mV s^{-1} in 0.6 M phosphate buffer, the onset of the catalytic current occurs at about –0.93 V, corresponding to an overpotential (applied potential minus thermodynamic potential for H_2 evolution at the same pH) of 0.52 V (Fig. 3a).

Controlled potential electrolysis (CPE) experiments were carried out in a double-compartment cell to assess the efficacy of catalyst **7**. As shown in Fig. 3b, the amount of charge used in 2 min increases with increasing overpotential until a saturation value of 0.43 C is reached at 0.64 V. This saturation behaviour occurs because the potential drop between the working and auxiliary electrodes exceeds the maximum output voltage of the potentiostat at high current densities, and is not an inherent property of the catalyst. Assuming, as validated below, that every electron is used for the reduction of protons, we also calculated the turnover frequency for the catalyst. The turnover frequency increases with overpotential, reaching a maximum of 1,600 moles of H_2 per mole of catalyst per hour (Fig. 3c). Control experiments performed using Na_2MoO_4 or $PY5Me_2$ showed no catalytic activity, and no catalytic activity was observed when fresh electrolyte was added to a used mercury electrode. Moreover, no solid deposits were observed on the mercury electrode, which remained shiny even after extended and repeated electrolysis experiments[20].

To optimize catalytic turnover frequency and to assess the long-term stability of compound **7**, we performed extended CPE experiments using a frit of greater diameter and a higher concentration of

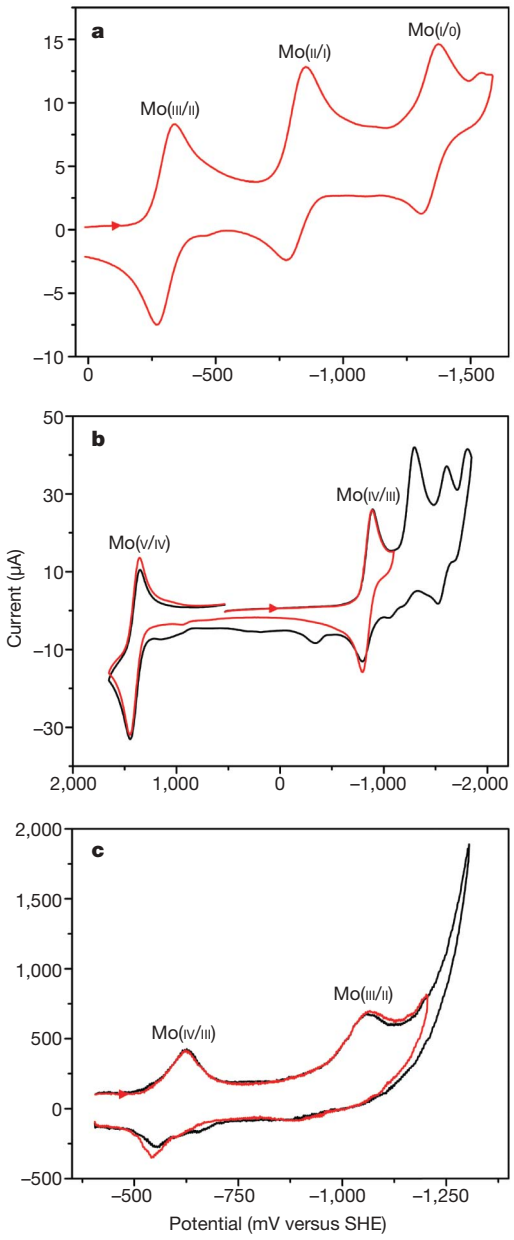

Figure 2 | Cyclic voltammograms of compounds 2 and 7. a, A 5 mM acetonitrile solution of **2**. **b**, A 2 mM acetonitrile solution of compound **7**. **c**, A 4.2 μM aqueous solution of compound **7**. Measurements in **a** and **b** were performed using 0.1 M $(Bu_4N)PF_6$ as the electrolyte with a scan rate of 100 mV s^{-1}, whereas the measurement in **c** was performed in 1 M KCl with a scan rate of 100 mV s^{-1}. In **b** and **c**, red lines indicate the initial scans and black lines indicate subsequent scans.

electrolyte to minimize internal resistance. Remarkably, the catalyst maintains activity under these conditions for at least 71 h, at which point the measurement was stopped because the concentration of hydroxide ions in the working electrode compartment overcame the capacity of the buffer. Thus, catalyst **7** is effective for long durations at close to neutral pH, with its durability apparently limited only by the strength of the buffer. The current levelled out at an average of 179(5) mA, (standard deviation given within parentheses) whereas a control experiment run under identical conditions, but without the catalyst, showed a current of just 1.1(1) mA. The charge accumulated over this period, after subtracting the contribution from the blank solution, resulted in a turnover number of 6.1×10^5 moles of H_2 per mole of catalyst with a turnover frequency of 8,500 moles of H_2 per mole of catalyst per hour (or 2.4 moles of H_2 per mole of catalyst per

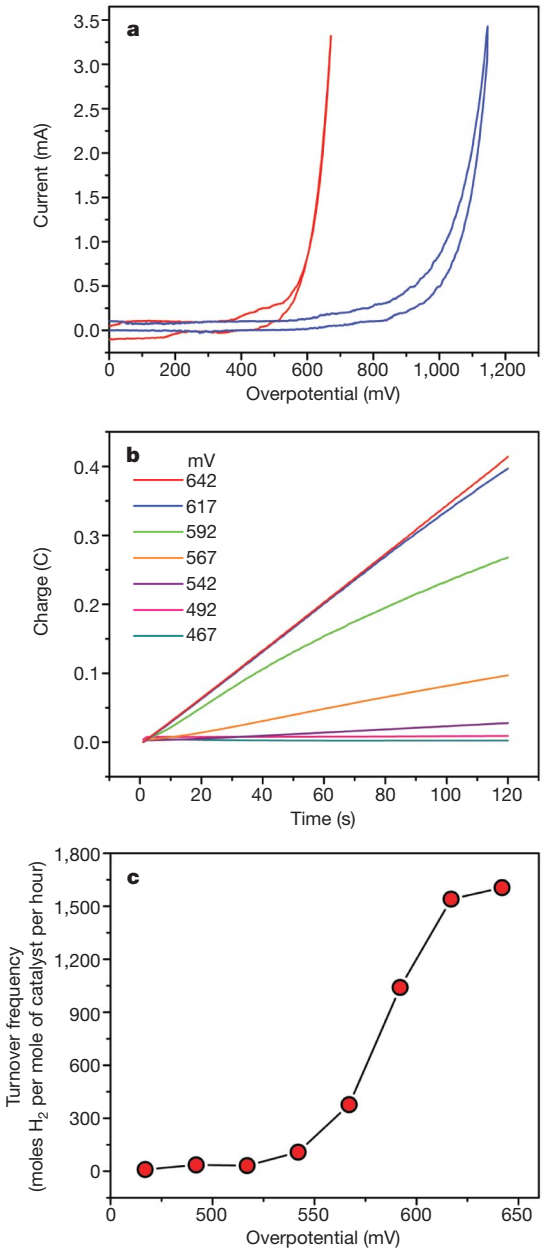

Figure 3 | Electrochemical data for a 7.7 μM solution of [(PY5Me$_2$)MoO](PF$_6$)$_2$ (7) in a 0.6 M phosphate buffer at pH 7. a, Cyclic voltammograms of the buffer with (red line) and without (blue line) compound **4** at a scan rate of 50 mV s^{-1}. **b**, Charge build-up versus time at various overpotentials. **c**, Turnover frequency versus overpotential. The background solvent activity has been subtracted from the plots in **b** and **c**. Overpotential = |applied potential minus E(pH 7)|. Turnover frequency calculations assume (see Supplementary Fig. 6) that every electron is used for the generation of hydrogen, and provide only a lower bound, given that not all catalyst molecules are in proximity to the electrode surface at a given time.

second) (Fig. 4). To the best of our knowledge, these values, which represent lower bounds, are significantly higher than any other reported molecular catalysts for electrochemical hydrogen production from neutral water, including a dinickel complex that exhibits a turnover number of 100 moles of H_2 per mole of catalyst with a turnover frequency of 160 moles of H_2 per mole of catalyst per hour at an overpotential of 820 mV (ref. 21) and a cobalt complex displaying a turnover number of 5 moles of H_2 per mole of catalyst with a turnover number of 0.4 moles of H_2 per mole of catalyst per hour at an overpotential of 390 mV (ref. 22). Further discussion of electrocatalysts that operate in organic as well as in acidic aqueous media is provided in the Supplementary Information.

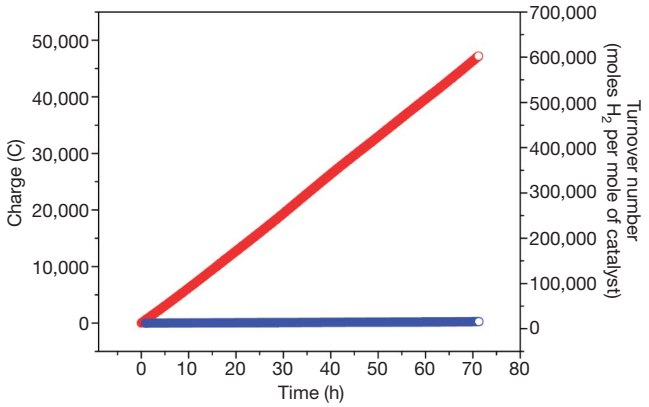

Figure 4 | Extended electrolysis. Electrolysis data for a 2 μM solution of [(PY5Me$_2$)MoO](PF$_6$)$_2$ (compound **7**) in a 3 M pH 7 phosphate buffer, showing charge build-up and turnover number versus time (red circles), and data for the buffer solution alone showing charge build-up versus time (blue circles) with the cell operating at a potential of −1.40 V versus SHE.

Assuming an application using such molecules would involve having them arranged in a single layer on the electrode surface, it is of interest to compare the performance of compound **7** with the hydrogenase enzymes on a per area basis[23]. Employing crystallographic unit cells, compound **7** exhibits an estimated footprint of 93 Å^2 per molecule, while hydrogenase enzymes occupy 5,400–12,000 Å^2 per molecule (Supplementary Information). Thus, packing together the number of molybdenum catalyst molecules needed to cover the area of a single hydrogenase protein can be expected to deliver a hydrogen production rate of 140–300 H_2 molecules per second, while also offering far greater stability.

To test the stability of compound **7** in the absence of a buffer, CPE experiments were performed in a 1 M aqueous KCl solution. Here, accumulation of hydroxide anions as H_2 is generated leads to an increase in pH. The accumulated charge within a given time period can be used to calculate the amount of H_2 produced, and, therefore, the concentration of OH^- ions in solution. Notably, the agreement between calculated and observed pH changes during 60 min of electrolysis (Supplementary Fig. 5) establishes that the catalyst indeed operates at Faradaic efficiency. Mass spectrometry studies indicate a reduced stability for $[(PY5Me_2)MoO]^{2+}$ at high pH, with a significant dissociation of the molybdenum centre from the $PY5Me_2$ ligand to generate $[MoO_4]^{2-}$ occurring above pH 12.

We also evaluated the catalytic performance in sea water, the Earth's most abundant proton source (Supplementary Fig. 6). On adding compound **7** to a sample of California sea water with no added electrolyte, the onset of catalytic current was observed at about –0.81 V versus SHE. In the absence of compound **7**, a catalytic current was not apparent until a potential of –1.60 V was attained. CPE experiments performed for short durations in sea water were remarkably similar to the results obtained in pH 7 buffered water. The current saturated at 0.32 C at an applied potential of –1.40 V versus SHE, corresponding to a turnover frequency of 1,200 moles of H_2 per mole of catalyst per hour at an overpotential of 0.78 V.

We tentatively propose the catalytic cycle depicted in Fig. 5 for the generation of hydrogen from water mediated by compound **7**. One-electron reduction of $[(PY5Me_2)MoO]^{2+}$ gives $[(PY5Me_2)MoO]^{1+}$, with addition of a second electron providing a putative $[(PY5Me_2)MoO]$ species. We note that the electrons are being added to orbitals that possess Mo $4d_{xz}/4d_{yz}$ character with π-type antibonding contributions from the oxo ligand. Reduction should weaken the Mo–O bond and enhance its nucleophilicity, enabling it to deprotonate nearby water molecules to produce the reactive intermediate $[(PY5Me_2)Mo(H_2O)]^{2+}$ and release two OH^- anions. Alternatively, each electron transfer step could be immediately followed by, or even coupled to, a proton transfer from water,

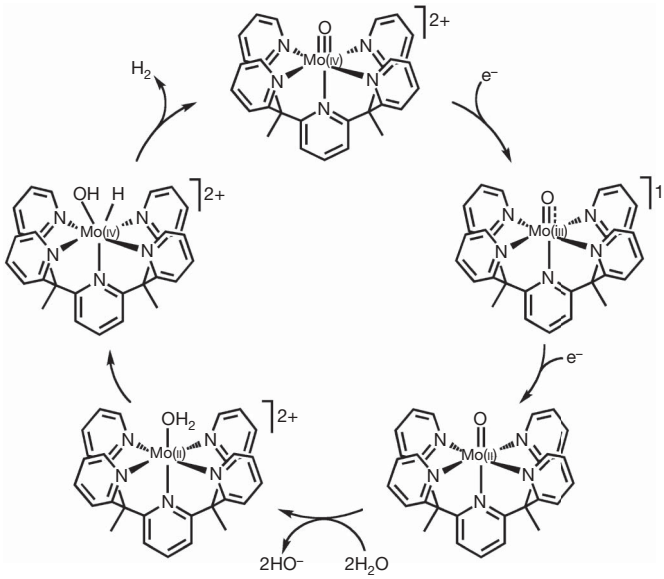

Figure 5 | Speculative electrocatalytic cycle for the reduction of water to release hydrogen and hydroxide anions. Although formal metal oxidation states are given for electron counting purposes, it should be recognized that there is probably significant delocalization of the added electrons onto the $PY5Me_2$ ligand. An alternative cycle, in which each reduction step is immediately followed by or even coupled to a proton transfer, is depicted in Supplementary Fig. 7.

giving rise to a cycle in which $[(PY5Me_2)Mo(OH)]^{2+}$ precedes the formation of $[(PY5Me_2)Mo(H_2O)]^{2+}$ (Supplementary Fig. 8). Although it is not widely used, ligand-centred proton reduction has been proposed as the basis for particular molecular catalysts that operate in acidic organic media[16,17], as well as for water reduction on MoS_2 surfaces[24,25]. Protonation of a bridging sulphido ligand has also been postulated in nitrogenase H_2 evolution[26]. The reduced aquo complex, $[(PY5Me_2)Mo(H_2O)]^{2+}$, in the present scheme could then eliminate H_2—perhaps in a manner akin to the reductive cleavage of water by $[(PY5Me_2)Mo(CF_3SO_3)]^{1+}$ (Fig. 1)—to regenerate $[(PY5Me_2)MoO]^{2+}$. One possible pathway for this last transformation would be via oxidative addition and α-abstraction[27–30].

Several observations are consistent with the above Mo(II)/Mo(IV) cycle. Under reductive catalytic conditions, CPE solutions of green catalyst **7** initially turn dark yellow and then change within 10 min to a purple-brown colour that is maintained for the remainder of the electrolysis (Supplementary Fig. 9). Once the potential was switched off, the solution quickly changed back to the dark yellow colour. Moreover, upon exposure to air, electrolysed solutions regenerate green $[(PY5Me_2)MoO]^{2+}$, as verified by ultraviolet-visual and infrared spectroscopy. We therefore speculate that a $PY5Me_2$ complex of Mo(II) is responsible for the reductive cleavage of water to release H_2 and OH^- ions.

The discovery of a molecular molybdenum-oxo catalyst for generating hydrogen from water without the use of additional acids and/or organic cosolvents establishes a new chemical paradigm for creating reduction catalysts that are highly active and robust in aqueous media. Ongoing efforts are focused on modifying $PY5Me_2$ and related platforms to further facilitate charge- and light-driven catalytic processes, with particular emphasis on chemistry relevant to sustainable energy cycles.

METHODS SUMMARY

Electrochemical methods. For the electrochemical studies we used a mercury pool working electrode with a surface area of 19.6 cm^2, which was stirred constantly during the CPE experiments. Electrical contact to the mercury pool was achieved through a platinum wire that remained immersed below the surface of the mercury, thereby avoiding contact with the solution. A 20.5 cm^2 platinum gauze (52 mesh, woven from 0.1-mm-diameter wire) was used as the auxiliary electrode and was separated from the solution in the working electrode compartment by a medium-porosity sintered-glass frit. The reference electrode was a commercially available aqueous Ag/AgCl electrode, which was positioned within 5 mm of the working electrode, and the potentials are reported with respect to SHE by adding 0.195 V to the experimentally obtained values. The working electrode compartment contained 5–100 ml of electrolyte solution, which was thoroughly sparged and kept under a blanket of water-saturated nitrogen during the experiments. Unless otherwise noted, a 0.6 M pH 7 phosphate buffer was used as electrolyte. Extended electrolyses lasting longer than an hour were conducted in a larger cell containing 170 ml of 1.8 M pH 7 phosphate buffer in each compartment. The solutions in both compartments were vigorously stirred during the electrolysis. Sea water was obtained from Ocean Beach, San Francisco, and was passed through a coarse paper filter before use to remove any particulate matter. *iR* (current times internal resistance) compensation was used in all experiments to account for the voltage drop between the reference and working electrodes using the software supplied with the BAS CV-50W cyclic voltammetry instrument.

The synthesis and characterization of new compounds are detailed in the Supplementary Information.

Received 17 November 2009; accepted 26 February 2010.

1. Lewis, N. S. & Nocera, D. G. Powering the planet: chemical challenges in solar energy utilization. *Proc. Natl Acad. Sci. USA* **103,** 15729–15735 (2006).
2. Turner, J. A. Sustainable hydrogen production. *Science* **305,** 972–974 (2004).
3. Du, P., Knowles, K. & Eisenberg, R. A homogeneous system for the photogeneration of hydrogen from water based on a platinum(II) terpyridyl acetylide chromophore and a molecular cobalt catalyst. *J. Am. Chem. Soc.* **130,** 12576–12577 (2008).
4. Fihri, A. *et al.* Cobaloxime-based photocatalytic devices for hydrogen production. *Angew. Chem. Int. Edn Engl.* **47,** 564–567 (2008).
5. Esswein, A. J. & Nocera, D. G. Hydrogen production by molecular photocatalysis. *Chem. Rev.* **107,** 4022–4047 (2007).
6. Tard, C. *et al.* Synthesis of the H-cluster framework of iron-only hydrogenase. *Nature* **433,** 610–613 (2005).
7. Sun, L., Åkermark, B. & Ott, S. Iron hydrogenase active site mimics in supramolecular systems aiming for light-driven hydrogen production. *Coord. Chem. Rev.* **249,** 1653–1663 (2005).
8. Frey, M. Hydrogen-activating enzymes. *ChemBioChem* **3,** 153–160 (2002).
9. Armstrong, F. A. Hydrogenases: active site puzzles and progress. *Curr. Opin. Chem. Biol.* **8,** 133–140 (2004).
10. Evans, D. J. & Pickett, C. J. Chemistry and the hydrogenases. *Chem. Soc. Rev.* **32,** 268–275 (2003).
11. Darensbourg, M. Y., Lyon, E. J., Zhao, X. & Georgakaki, I. P. The organometallic active site of [Fe]hydrogenase: models and entatic states. *Proc. Natl Acad. Sci. USA* **100,** 3683–3688 (2003).
12. Gloaguen, F. & Rauchfuss, T. B. Small molecule mimics of hydrogenases: hydrides and redox. *Chem. Soc. Rev.* **38,** 100–108 (2009).
13. Felton, G. A. N. *et al.* Hydrogen generation from weak acids: electrochemical and computational studies of a diiron hydrogenase mimic. *J. Am. Chem. Soc.* **129,** 12521–12530 (2007).
14. Baffert, C., Artero, V. & Fontecave, M. Cobaloximes as functional models for hydrogenases. 2. Proton electroreduction catalyzed by difluoroborylbis-(dimethylglyoximato)cobalt(II) complexes in organic media. *Inorg. Chem.* **46,** 1817–1824 (2007).
15. Hu, X., Brunschwig, B. S. & Peters, J. C. Electrocatalytic hydrogen evolution at low overpotentials by cobalt macrocyclic glyoxime and tetraimine complexes. *J. Am. Chem. Soc.* **129,** 8988–8998 (2007).
16. Wilson, A. D. *et al.* Hydrogen oxidation and production using nickel-based molecular catalysts with positioned proton relays. *J. Am. Chem. Soc.* **128,** 358–366 (2006).
17. Appel, A. M., DuBois, D. L. & DuBois, M. R. Molybdenum-sulfur dimers as electrocatalysts for the production of hydrogen at low overpotentials. *J. Am. Chem. Soc.* **127,** 12717–12726 (2005).
18. Goldsmith, J. I., Hudson, W. R., Lowry, M. S., Anderson, T. H. & Bernhard, S. Discovery and high-throughput screening of heteroleptic iridium complexes for photoinduced hydrogen production. *J. Am. Chem. Soc.* **127,** 7502–7510 (2005).
19. Klein Gebbink, R. J. M., Jonas, R. T., Goldsmith, C. R. & Stack, T. D. P. A periodic walk: a series of first-row transition metal complexes with the pentadentate ligand PY5. *Inorg. Chem.* **41,** 4633–4641 (2002).
20. Jaksic, M. M. & Csonka, I. M. Acceleration of sodium amalgam decomposition by depolarization with molybdenum graphite in the mercury cell process. *Electrochem. Technol.* **4,** 49–56 (1966).
21. Collin, J. P., Jouaiti, A. & Sauvage, J. P. Electrocatalytic properties of $Ni(cyclam)^{2+}$ and $Ni_2(biscyclam)^{4+}$ with respect to carbon dioxide and water reduction. *Inorg. Chem.* **27,** 1986–1990 (1988).

22. Bernhardt, P. V. & Jones, L. A. Electrochemistry of macrocyclic cobalt(III/II) hexaamines: electrocatalytic hydrogen evolution in aqueous solution. *Inorg. Chem.* **38,** 5086–5090 (1999).
23. Armstrong, F. A. *et al.* Dynamic electrochemical investigations of hydrogen oxidation and production by enzymes and implications for future technology. *Chem. Soc. Rev.* **38,** 36–51 (2009).
24. Hinnemann, B. *et al.* Biomimetic hydrogen evolution: MoS_2 nanoparticles as catalyst for hydrogen evolution. *J. Am. Chem. Soc.* **127,** 5308–5309 (2005).
25. Jaramillo, T. F. *et al.* Identification of active edge sites for electrochemical H_2 evolution from MoS_2 nanocatalysts. *Science* **317,** 100–102 (2007).
26. Dance, I. The hydrogen chemistry of the FeMo-co active site of nitrogenase. *J. Am. Chem. Soc.* **127,** 10925–10942 (2005).
27. Yoon, M. & Tyler, D. R. Activation of water by permethyltungstenocene; evidence for the oxidative addition of water. *Chem. Commun.* 639 (1997).
28. Blum, O. & Milstein, D. Oxidative addition of water and aliphatic alcohols by $IrCl(trialkylphosphine)_3$. *J. Am. Chem. Soc.* **124,** 11456–11467 (2002).
29. Ozerov, O. V. Oxidative addition of water to transition metal complexes. *Chem. Soc. Rev.* **38,** 83–88 (2009).
30. Kohl, S. W. *et al.* Consecutive thermal H_2 and light-induced O_2 evolution from water promoted by a metal complex. *Science* **324,** 74–77 (2009).

Supplementary Information is linked to the online version of the paper at www.nature.com/nature.

Acknowledgements We acknowledge the NSF (grant number CHE-0617063) for research funding in the initial stages of this project. For the later stages, we acknowledge the Helios Solar Energy Research Center, which is supported by the Office of Science, Office of Basic Energy Sciences of the US Department of Energy under contract number DE-AC02-05CH11231. C.J.C. is an Investigator with the Howard Hughes Medical Institute. We thank Tyco Electronics for the partial support of H.I.K. We also thank M. Majda for discussions, D. M. Jenkins and P. Dechambenoit for experimental assistance, A. T. Iavarone for obtaining the mass spectra, and J. D. Breen for fabrication of the electrochemical cells.

Author Contributions H.I.K., C.J.C. and J.R.L. planned the research, and H.I.K. performed the experiments. H.I.K., C.J.C. and J.R.L. prepared the manuscript.

Author Information X-ray coordinates from the crystal structure determinations have been deposited with the Cambridge Crystallographic Data Centre with reference codes 720362 (compound **1**), 720363 (compound **2**), 753993 (compound **5**), 753992 (compound **6**) and 720364 (compound **7**). Reprints and permissions information is available at www.nature.com/reprints. The authors declare no competing financial interests. Readers are welcome to comment on the online version of this article at www.nature.com/nature. Correspondence and requests for materials should be addressed to C.J.C. (chrischang@berkeley.edu) or J.R.L. (jrlong@berkeley.edu).